A PLANAR VECTOR MODEL OF COLOR VISION AND THE APPLICATION OF ITS COLOR SPACE TO COLOR REPRODUCTION

James R. Huntsman*

Abstract

A new color space for color reproduction is developed from an empirical model of color vision based on a trigonally symmetric, planar arrangement of three response vectors, which separates a visual perception via tristimulus values into achromatic and chromatic components and subsequently recombines them as a correlate of purity visually. Since three visual response vectors are mutually opposed, the model is called the mutually opposed, trichromatic response (MOTR) model. The MOTR model predicts many visual responses such as unique hues, wavelength discrimination, and defective color vision. Since the model has the advantage of directly representing a color as two chromatic components and one achromatic component, it is particularly useful for halftone color reproduction, especially via complete GCR.

Introduction

Most color models are based on the three-receptor (trichromatic) response model of Young [1], Maxwell [2-5], and von Helmholtz [6, 7], or on the opponent response model of Hering [8]. Present models tend to combine both these models into what is called a zone theory [9, 10], where the characteristics of both trichromatic and opponent response can operate in different stages. A prevalent characteristic is that the visual stimulus is separated into luminance (lightness or brightness) and chromatic ("color") components. The chromatic component further comprises the two characteristics of hue (red, green, etc.) and chroma.

* Printing & Publishing Systems Div./3M Co.
St. Paul, Minnesota 55144

There are linear [11] and nonlinear response models, the latter including vector models [9, 10, 12, 13, 45]. Vector models invariably are based on a mutually orthogonal Cartesian coordinate system, likely for simplicity. However, from crystallography, it is obvious that Nature seldom uses a coordinate system of such symmetry. The object of this paper is to propose a model based on a symmetrical, planar arrangement of three vectors, each representing the overall response of the three conal systems ("red", "green", and "blue"). The psychophysical basis will be only that equal response of the three conal systems results in an achromatic response and that a chromatic response is due to unequal response of these conal systems. A principal characteristic of the model, similar to other models, is that the visual response is separated into achromatic and chromatic responses. Also presented will be a color space for surface colors which allows a quantitative measure of color differences. A second characteristic of the model is that it utilizes aspects of existing color models and spaces in a uniquely different way. The overall objective herein is to provide a simple yet sufficiently accurate model which will be useful for colorimetric analysis and application to color reproduction, the halftone proofing and printing processes in particular. Some familiarity with the CIE color systems is assumed.

CIE Color Systems

The starting point for the CIE's visual response and color space systems is the color matching-functions of a "standard observer". The 1931 and 1964 CIE Standard Observer functions are similar but differ in the "blue" function and the luminous efficiency function. Since this paper is directed toward the graphic arts, and the graphic arts usually uses "wide field" viewing, the development herein will be based on the CIE 10° color-matching functions unless otherwise noted. Where used, they will be designated $\bar{x}_{10}$, $\bar{y}_{10}$, and $\bar{z}_{10}$.

The next step in describing a visual response is quantifying the response, which is usually done by calculating X, Y, and Z, the CIE tristimulus values for that response. The 1931 CIE chromaticity diagram is based on the proportion of each tristimulus value to their total, giving chromaticity coordinates as described in equation (1).

$$x = \frac{X}{X+Y+Z} \qquad y = \frac{Y}{X+Y+Z} \qquad z = 1-x-y \qquad (1)$$

A plot of the monochromatic visible spectrum in CIE x,y chromaticity coordinates is given in Fig. 1, the familiar "horseshoe". The white point is located at X =Y= Z, or $x = y = z = 1/3$. The normal direction is given by the Y tristimulus value, which correlates with perceived lightness. This system is usually designated xyY.

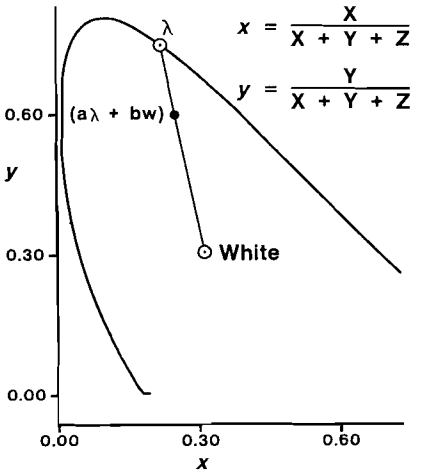

Fig. 1. 1931 CIE chromaticity diagram of the visible spectrum.

A big deficiency in using chromaticity coordinates and Fig. 1 is that the approach does not correlate well with the appearance of colors, especially surface colors. Perhaps one reason for this deficiency is the characteristics of this approach. In this approach, the X, Y, and Z values represent imaginary, not real stimuli, and x, y, and z represent the fractional contributions of these imaginary stimuli. The most unusual, if not irrational, aspect of these imaginary stimuli is that the X and Z stimuli are considered to contribute no luminance, and all luminance is provided solely by the Y stimulus. This implies that stimuli having no luminance can contribute to a visual perception. Although imaginary characteristics may be permiss-

ible for modeling, such characteristics tend to impair conceptualization of real processes.

To investigate the characteristics of the CIELAB and CIELUV systems, ideal yellow (Y), magenta (M), cyan (C), red (R), green (G), blue (B), and white (W) colors can be used since their behavior can be predicted readily. Their reflectance is either 0 or 1 in their appropriate part of the visible spectrum. That is, Y, M, and C comprise 2/3 of the spectrum, while R, G, and B comprise 1/3. White comprises exactly the sum of R, G, and B. MacAdam [14, 15] called these optimum object stimuli since they represented the boundaries of real colors. All spectral related data used herein for these ideal colors range from 380 nm to 720 nm in 5 nm intervals.

In the halftone process, tone reproduction and gray balance are requisite, not merely important, and it is highly desirable that hue doesn't change throughout the tone reproduction curve. Hue constancy throughout a gradation scale can be estimated by the hue angle h_{ab} or h_{uv}. Since ideal colors are being used in conjunction with a standard observer, there should be no shift in its hue in any color space. This does not mean there would not be a perceived hue shift for real observers.

The reflectance spectrum of an ideal yellow is shown in Figures 2 and 3, where the solid line defines the spectrum of the ideal yellow. Fig. 2 represents the usual case in halftone printing via the subtractive color process, where the starting point is a white substrate such as paper. If that substrate is an ideal white, its reflectance is 1 throughout the spectrum. As the amount of colorant (ink) is increased through higher density or dot area, it "subtracts" (absorbs) the wavelengths from an appropriate part of the spectrum.

In Fig. 2, then, the dashed lines represent the contribution of an ideal white base as a converse function of the dot area of the yellow colorant. In particular, since ideal materials are involved, the reflectance level for the dashed line is the fractional dot area of the white substrate. An alternative perspective is that since white comprises yellow and its complementary color blue, the decreasing level of reflectance of the dashed lines represents the "removal" of blue from that spectral region by increasing the amount of the yellow colorant which subtracts blue.

In Fig. 3, the dashed lines represent the result of discrete addition of an ideal black to the ideal yellow already at 100% coverage. The decreasing levels of the yellow's maximum reflectance represent the effect of increasing dot area of the black. Alternatively, it can represent the effect of the colorant on papers of various uniform gray levels. Table 1 gives numerical data for hab, huv, and the uniform reflectance R(B) for the complementary levels of ideal blue (B) in Fig. 2. Table 2 gives similar data for Fig. 3.

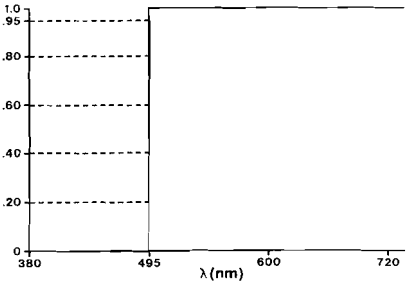

Fig. 2. Reflectance of unit halftone as a function of dot area of ideal yellow on an ideal white substrate.

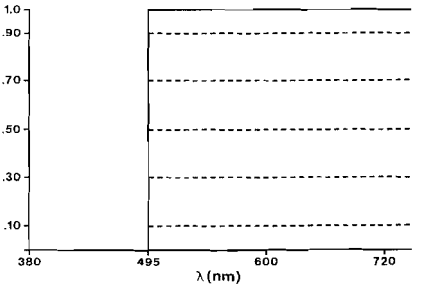

Fig. 3. Reflectance of unit halftone area having 100% ideal yellow as a function of dot area of an added ideal black.

Table 1

Reflectance R(B), % Dot Areas, and Hue Angles for Fig. 2.

R(B)	%W/%Y	hab	huv
0.95	95/5	102.85	79.14
0.80	80/20	102.31	79.14
0.60	60/40	101.48	79.14
0.40	40/60	100.47	79.14
0.20	20/80	99.12	79.14
0.00	0/100	96.81	79.14

Table 2

Reflectance (R) and Hue Angles for Fig. 3.

R	hab	huv
1.0	96.81	79.14
0.9	96.81	79.14
0.5	96.81	79.14
0.3	96.81	79.14
0.1	94.68	79.14

%W/%Y = ratio of % dot area of white base (W) to % dot area of yellow (Y)

As can be seen from Tables 1 and 2, there is an anomaly in the hue angle h_{ab} of CIELAB, but not for h_{uv} of CIELUV. The value of h_{ab} ranged over six degrees for the tint scale represented in Fig. 2. However, for the shade scale represented in Fig. 3, h_{ab} shifted only at a low reflectance level. Anomalies in h_{ab} at very small tristimulus values have been discussed by McLaren [16]. Data for ideal magenta and cyan are similarly given in Table 3.

Table 3

Reflectance (R), % Dot Areas, and Hue Angles for Ideal Magenta (M) and Cyan (C) Spectra Equivalent to Those in Fig. 2.

R	%W/%M	h_{ab}(M)	h_{uv}(M)	%W/%C	h_{ab}(C)	h_{uv}(C)
0.95	95/5	308.67	289.95	95/5	198.09	189.15
0.80	80/20	309.45	289.95	80/20	197.86	189.15
0.60	60/40	310.69	289.95	60/40	197.52	189.15
0.40	40/60	312.26	289.95	40/60	197.17	189.15
0.20	20/80	314.32	289.95	20/80	196.80	189.15
0.00	0/100	317.26	289.95	0/100	196.41	189.15

Unlike the data in Table 2 for black added to yellow, there was no change in the hue angles for ideal magenta and cyan, so those data are not given in Table 3. While the anomaly for ideal yellow at very small tristimulus values would seldom be of concern in halftone printing, the behavior of h_{ab} throughout a tint scale as depicted in Fig. 2 could be relevant to halftone printing since such scales are quite the norm. The shift in h_{ab} is 9° for magenta while the shift is only 2° for cyan. In practice, this behavior might either enhance or offset the colorimetric values of a normal ink so that a colorimetric representation of the ink would not be consistent with the visual perception of the ink. This anomaly did not occur for h_{uv} in the CIELUV system.

The various colorimetric parameters for ideal primary and secondary colors are given in Table 4. Plots of tint scales in 10% dot area increments of these ideal colors are given in Figures 4 and 5. It can be seen in Fig. 4 that in CIELAB the lines of constant hue are curved as is well known; whereas, in CIELUV, Fig. 5, the hue lines are straight. In Fig. 4, there is a great distortion at 100% red (R), due likely to $Z = 0$. Although complementary colors in Fig. 5 are

"opposite", the radial spacings, especially for cyan and red, are not symmetrically uniform, suggesting incorrectly that solid red and cyan would not add (graphically) to a neutral at the origin.

Table 4

CIELUV and CIELAB Parameters for
Ideal Primary and Secondary Colors

Color	L*	u*	v*	C*uv	huv	a*	b*	C*ab	hab
Y	96.45	20.85	108.69	110.67	79.14	-14.64	122.60	123.47	96.81
M	53.58	44.81	-123.44	131.32	289.95	83.30	-76.96	113.41	317.26
C	94.88	-48.75	-7.85	49.38	189.15	-30.00	-8.83	31.27	196.41
R	42.27	167.39	26.96	169.55	9.15	76.37	100.46	126.20	52.76
G	90.97	-40.05	110.32	117.36	109.95	-51.48	113.16	124.32	114.46
B	35.81	-25.92	-135.10	137.56	259.14	53.21	-107.60	120.04	296.31

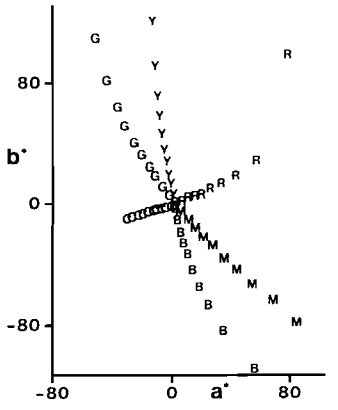

Fig. 4. Ideal Y,M,C,R,G, & B 10% tint scales in CIELAB.

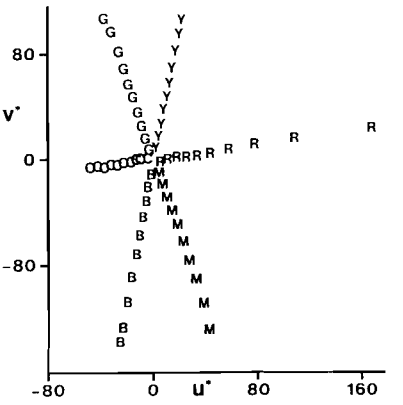

Fig. 5. Ideal Y,M,C,R,G, & B 10% tint scales in CIELUV.

The Psychophysical Model

Although the model herein is unique, it has a conceptual basis similar to the CIE color spaces. First, equal response of the conal

systems results in "white". Second, consider the fact that one sees a color hue with monochromatic light even in regions where the three conal systems are simultaneously stimulated (*e.g.*, green). This could suggest that the total visual stimulation can be separated into two components: an achromatic one ("white") and a chromatic one (hue, chroma). Also, color stimuli can be added to form a new color stimulus with its own achromatic and chromatic components. The achromatic component corresponds to the smallest tristimulus value, which can be X, Y, or Z, depending on the color. In the calculation of the tristimulus values, this is equivalent to letting the reflectance $R(\lambda)$ comprise a constant value R_0 plus a variable value $R'(\lambda)$. It is analogous in electrical circuit theory to superimposing an AC voltage on a DC voltage.

The tristimulus values for the ideal colors in Table 4 are given in Table 5, where W indicates the "white" (achromatic) component in that particular color. With regard to secondary colors, it is seen that, for example, X(R) = X(Y) + X(M) - X(W), etc., for X(G), X(B), and likewise for Y(R, G, B) and Z(R, G, B). Note that the sum of either the primaries or the secondaries produces equal tristimuli, or white, as does the addition of a primary and its complement. The reason for some values not equaling exactly 100.000 is due to limiting the visible spectrum to 380 nm to 720 nm, which truncates more red and green than blue standard observer values. The mathematical agreement is very good, and three decimal places are used only because all theoretical values are used. In practice with real colors, one decimal place is more than sufficient.

For subtractive mixing, the white component, W, is simply subtracted from all the tristimulus values, since in subtractive mixing, regions are subtracted by absorption from a white base to leave a net color stimulation. For subtractive mixing, the primaries can be reduced to "net" chromatic tristimuli by subtracting out each's white component. Then, resultant hues can be determined from linear combinations of the reduced primaries. Net chromatic tristimuli are given in Table 6, derived from Table 5. It is seen in Table 6 that for net chromatic stimuli, each net color (Y", M", C", R", G", B") has one zero tristimulus value, but that zero tristimulus value is derived from a different W for each color.

Table 5

Tristimulus and White (W) Component Values For Ideal Colors

Color	X	Y	Z	W
Y	83.059	91.089	4.526	4.526
M	45.016	21.586	95.492	21.586
C	71.871	87.325	100.017	71.871
R	28.102	12.675	0.000	0.000
G	54.957	78.414	4.526	4.526
B	16.914	8.911	95.492	8.911
Y+M+C	199.946	200.000	200.035	199.946
R+G+B	99.973	100.000	100.018	99.973
Y +M	128.075	112.675	100.018	100.000
Y +C	154.930	178.414	104.543	100.000
M+C	116.887	108.911	195.509	100.000
Y +M - W	28.075	12.675	0.018	0.018
Y + C - W	54.930	78.414	4.543	4.543
M+ C - W	16.887	8.911	95.509	8.911
R+G	83.059	91.089	4.526	4.526
G+B	71.871	87.325	100.017	71.871
B+R	45.016	21.586	95.492	21.586
Y +R	99.973	100.000	100.018	99.973
M+G	99.973	100.000	100.018	99.973
C +R	99.973	100.000	100.018	99.973

A fundamental principle of this model, like other models, is that if unequal X, Y, and Z lead to chroma and hue, the visual system might initially separate the achromatic and chromatic components of a given stimulus and then subsequently recombine them. An orthogonal XYZ vector system will not directly accomplish this separation. Instead, to represent such a separation, a trigonally (120°) symmetric, planar arrangement of vectors is proposed as shown in Fig. 6, where each conal system's total response, corre-

lated with its tristimulus value, is fed to a vector-like channel, mutually opposing the other two in a dynamic counterbalance fashion, not unlike the opposing flexor-extensor counterbalance of the neuromuscular system.

Table 6

Net Chromatic Tristimuli For Ideal Colors

Color	X"	Y"	Z"
Y" [=Y -W(Y)]	78.533	86.563	0.000
M"[=M-W(M)]	23.430	0.000	73.906
C" [=C-W(C)]	0.000	15.454	28.146
R"[=R-W(R)]	28.102	12.675	0.000
G"[=G-W(G)]	50.431	73.888	0.000
B"[=B-W(B)]	8.003	0.000	86.581
Y"+M"	101.963	86.563	73.906
Y"+M"-W(Y"+M")	28.057	12.657	0.000
Y"+C"	78.533	102.017	28.146
Y"+C"-W(Y"+C")	50.387	73.871	0.000
M"+C"	23.430	15.454	102.052
M"+C"-W(M"+C")	7.796	0.000	86.598
Y"+M"+C"	101.963	102.017	102.052
Y"+M"+C"-W(Y"+M"+C")	0.000	0.054	0.089
R"+G"+B"	86.536	86.563	86.581
R"+G"+B"-W(R"+G"+B")	0.000	0.027	0.045
Y"+B"	86.536	86.563	86.581
M"+G"	73.861	73.888	73.906
C"+R"	28.102	28.129	28.146

This type of graphical arrangement *per se* is not a new way to represent tristimulus values and is somewhat analogous to GATF's density color hexagon determination. However, this arrangement

has not yet been fully developed as a visual vector model. This vector arrangement is simultaneously consistent with both the Young-Helmholtz trichromatic and Hering opponent models. It has three independent responses, and each response is mutually "opposed" to the other two. It will, therefore, be called the mutually opposed, trichromatic response (MOTR) model.

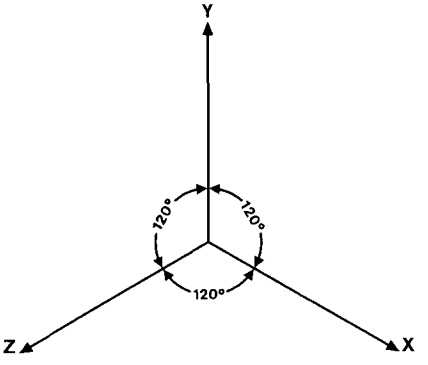

Fig. 6. Symmetrical planar arrangement of tristimulus vectors.

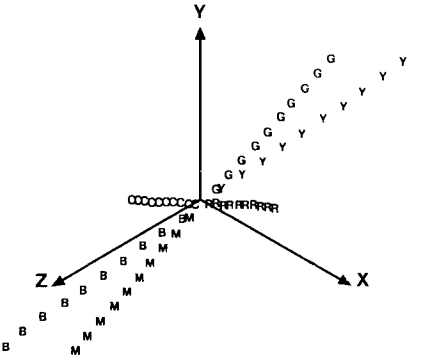

Fig. 7. 10% tint scales of ideal colors according to the MOTR model.

However, the model cannot be best utilized as shown in Fig. 6. For the moment, it can be used to plot the ideal colors as was done in Figures 4 and 5. If the X, Y, and Z values of the ideal colors are plotted in this way, Fig. 7 results. Note that the complementary colors are exactly 180° opposite and equally spaced, guaranteeing that if they are added vectorially, "white" will be produced. However, their angular spacing is not uniform, as might be desired. It would be aesthetically nice if they plotted as a hexagon; however, it is not a colorimetric requirement that a hexagon should be produced, although one can be with a suitable transformation. It can be seen that in a planar arrangement, a mutual angle of 120° provides the largest overall color gamut.

To better understand the model, it will be developed first for the visual response to the monochromatic spectrum. The CIE 10° Standard Observer color-matching functions will be treated as if they are tristimulus values. In Fig. 8, let $\bar{x}_{10}$, $\bar{y}_{10}$, and $\bar{z}_{10}$ represent the value of the CIE 10° Standard Observer color-matching functions at

a given wavelength, and **C** the MOTR model chromaticity vector resulting from those functions according to vector equation (2). Bold letters will represent a vector. Theta (θ) is the counterclockwise angle between the **X** axis and the chromaticity vector **C**, and represents the hue of **C**. The magnitude of **C**, $|\mathbf{C}|$, from planar trigonal coordinates, is given in (3) and represents MOTR chroma C.

$$\mathbf{C} = \bar{x}_{10}\mathbf{X} + \bar{y}_{10}\mathbf{Y} + \bar{z}_{10}\mathbf{Z} \tag{2}$$

$$|\mathbf{C}|^2 = \bar{x}_{10}^2 + \bar{y}_{10}^2 + \bar{z}_{10}^2 - \bar{x}_{10}\bar{y}_{10} - \bar{x}_{10}\bar{z}_{10} - \bar{y}_{10}\bar{z}_{10} \tag{3}$$

From Fig. 8, it can be seen that the effect of this vector geometry is to subtract the smallest value of $\bar{x}_{10}$, $\bar{y}_{10}$, and $\bar{z}_{10}$ from the other two. The case depicted in Fig. 8 is for $\bar{y}_{10} > \bar{x}_{10} > \bar{z}_{10}$, but holds for any relation. The representation of **C** in (2) can be rewritten as in (4), and thus as in (5), where $x' = (\bar{x}_{10} - w)$; $y' = (\bar{y}_{10} - w)$; $z' = (\bar{z}_{10} - w)$ ($z' = 0$ in this case); and w is the smallest of $\bar{x}_{10}$, $\bar{y}_{10}$, and $\bar{z}_{10}$.

Note that if $\bar{x}_{10} = \bar{y}_{10} = \bar{z}_{10}$, the resultant point is zero, the origin (achromatic point). If $\bar{x}_{10}$, $\bar{y}_{10}$, and $\bar{z}_{10}$ are unequal, the resultant vector will be a point away from the origin, having hue and chroma. It is seen that the effect of the vector addition of the smallest tristimulus value, if non-zero, to a first vector resulting from the vector addition of the two larger tristimulus values is to reduce the magnitude of the first vector, and to change its direction (hue) unless the first vector is 180° from the smallest tristimulus value's axis. For purposes of angular designation, the **X** axis is taken as the reference.

$$\mathbf{C} = (\bar{x}_{10} - w)\mathbf{X} + (\bar{y}_{10} - w)\mathbf{Y} + (\bar{z}_{10} - w)\mathbf{Z} \tag{4}$$

$$\mathbf{C} = x'\mathbf{X} + y'\mathbf{Y} + z'\mathbf{Z} \tag{5}$$

The angle θ is defined from vector algebra as in (6), or it can also be determined after transformation to Cartesian coordinates.

$$\cos\theta = \frac{\mathbf{X} \bullet \mathbf{C}}{|\mathbf{X}|\,|\mathbf{C}|} \tag{6}$$

A plot of **C** for $\bar{x}_{10}$, $\bar{y}_{10}$, and $\bar{z}_{10}$ from 400 nm to 700 nm in 5 nm intervals is given in Fig. 9. The shape in Fig. 9 is a planar equivalent of that plotted by Adams [17 (Fig. 2)] in orthogonal tristimulus space according to his theory of color vision [18].

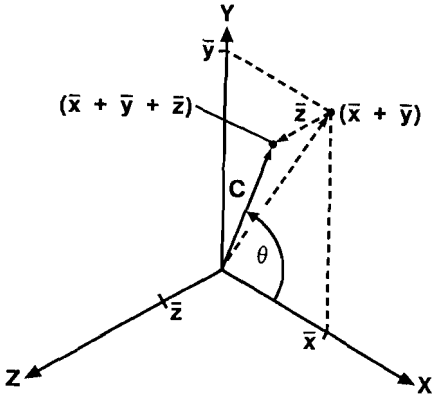

Fig. 8. Mapping of CIE 10° color-matching functions according to the MOTR model.

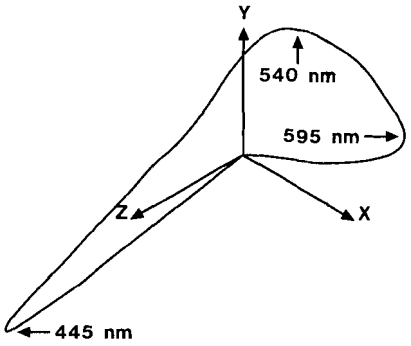

Fig. 9. CIE 10° color-matching functions according to the MOTR model.

While Fig. 9 represents the chroma of the spectral wavelengths, in doing so it somewhat disguises the model's hue characteristics of the spectrum. Since hue is due to the relative proportions of chromatic stimuli, one can transform Fig. 9 to a qualitative hue diagram by making the stimuli (x', y', z') relative to the absolute response sensitivity scales along **X**, **Y**, and **Z** through proportionalization. To proportionalize x', y', and z' with respect to **X**, **Y**, and **Z**, one merely needs to divide each by their sum. This is equivalent to the calculation of the 1931 CIE chromaticity coordinates. Thus, the proportionalized chroma vector, **C**", can be given by (7).

$$\mathbf{C}'' = \frac{\mathbf{C}}{x' + y' + z'} = x''\mathbf{X}'' + y''\mathbf{Y}'' + z''\mathbf{Z}'' \qquad (7)$$

where $x'' = x'/(x'+y'+z')$, $y'' = y'/(x'+y'+z')$, $z'' = z'/(x'+y'+z')$

Since vector **C** is divided by a scalar, the direction θ of **C** and **C**"are identical, but **C**" is always smaller in magnitude. By making the vector components proportional, the axes can be thought of as unit normalized. Thus, in effect, $|\mathbf{X}''| = |\mathbf{Y}''| = |\mathbf{Z}''| = 1$. If Fig. 9 is replotted as **C**" according to (7), Fig. 10 results.

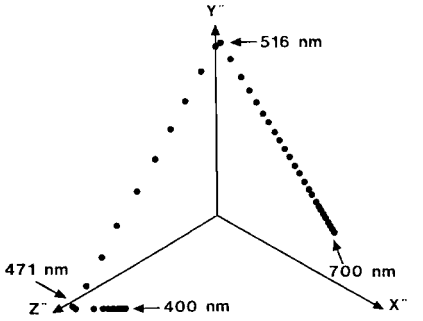

Fig. 10. Spectrum when plotted as proportionalized vectors according to the MOTR model.

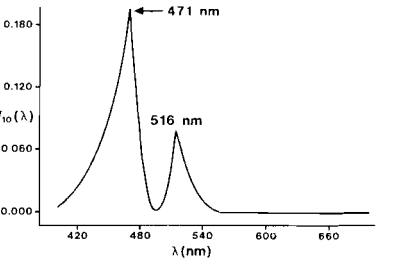

Fig. 11. White component W of the spectrum according to the MOTR model.

That a straight sided triangle should result is most desirable, for it represents any hue as a mixture of the hues at the apices [(1,0,0), (0,1,0), (0,0,1)], which are unique hues. White is at the center (0,0,0). It is similar to Maxwell's triangle but has the property of predicting the perceptually unique hues directly from its geometry. The wavelength of unique green would be at the vertical apex (θ = 120°) and is 516 nm. Unique blue would be at the lower left apex (θ = 240°) and is 471 nm. The hue yellow would be at θ = 60°, where x" = y", which is the wavelength where the $\bar{x}_{10}$ and $\bar{y}_{10}$ color-matching functions are equal; *i.e.*, at about 573 nm. These wavelengths for unique hues are consistent with those of Dimmick and Hubbard [19]. Although the 1931 CIE chromaticity diagram suggests an apex in the vicinity of 515 - 520 nm, it does not suggest where unique blue is unless the position of yellow is first defined. The curvature in the *xy*Y system is due to including the achromatic contributions in both the numerator and denominator rather than treating them separately. These unique hues occur in Fig. 9 at the same θ, *e.g.*, where the chroma locus intersects the **Y** and **Z** axes.

According to Fig. 10, there is no monochromatic unique red (θ = 0°), but rather unique red is from mixing long wavelength red with

some blue. It is emphasized that according to the MOTR model, the lack of a unique monochromatic red is not due to insufficient conal sensitivity in the far red, but rather is due to the green color-matching function being greater than zero at the long wavelength end of the spectrum. In this model, unique hues occur where the two smaller color-matching functions are equal, making two of x", y", z" equal zero. Thus, a monochromatic red would require green and blue functions to be zero while red was reasonably finite within the visible spectrum. Although in standard tables, $\bar{y}_{10}$ does go to zero at 760 nm while $\bar{x}_{10}$ is 0.0001, such a distinction is more mathematical than psychophysical. In the MOTR model, unique red is determined by its complementary wavelength ($\theta = 180°$), which is at about 492 nm, and which agrees closely with the value of Dimmick and Hubbard [20] of 494 nm. This value is also a neutral point for protanopes. If this model is applied to the conal sensitivities of Smith and Pokorny [21] or Estevez [22], as have models based on them by Boynton [23] and Hunt [24, 25], all the psychologically unique hues are not determined. Also, these models do not directly predict unique blue as the MOTR model easily does, even though they involve extensive mathematical manipulations. Although beyond this paper's scope, the MOTR model describes well the defective color vision characteristics of protanopia, deuteranopia, and tritanopia by simply allowing the appropriate color-matching function to be zero for all wavelengths and proceeding as before.

Although the CIE *xy*Y system also utilizes proportional amounts of the tristimulus values to arrive at both hue and purity, the principal difference of the MOTR model is that only the portions of the tristimulus values which contribute to chromaticity are utilized. In the CIE *xy*Y system, the spectrum locus defines 100% excitation purity at all wavelengths. In the MOTR model, "excitation purity" (*i.e.*, purity of the visual *response*) is not the same for all wavelengths. MOTR excitation purity is 100% only where $|\mathbf{W}| = 0$. In regions where $\bar{x}_{10}$, $\bar{y}_{10}$, and $\bar{z}_{10}$ are all nonzero, $|\mathbf{W}| > 0$, so purity < 100%. Since hue derives from proportions of $\bar{x}_{10}$, $\bar{y}_{10}$, and $\bar{z}_{10}$ in the visual response, Fig. 10 is a hue diagram and not a chromaticity diagram because it is not based on chroma.

An appearance response, **A**, can, therefore, be thought of as the mixed sum of chromatic and achromatic vectors according to (8), where the coefficient "a" would correlate with the luminous efficiency function. Since appearance includes the three perceptions of hue,

lightness, and purity, lightness (and brightness) includes both achromatic and chromatic contributions and would correlate with $|\mathbf{A}|$, which would correlate with luminance. For qualitative purposes, it is the proportion of $|\mathbf{W}|$ and $|\mathbf{C}|$ that would correlate with purity. This is similar in concept to the CIE *xy*Y diagram, where a point is considered a mixture of a pure chromatic component and a white (achromatic) component. The correlate of the proportion of $|\mathbf{C}|$ to the sum of $|\mathbf{C}|$ and $|\mathbf{W}|$ is purity (P) as given in (9).

$$\mathbf{A} = a\mathbf{C} + b\mathbf{W} \tag{8}$$

$$P = \frac{|\mathbf{C}|}{|\mathbf{C}| + |\mathbf{W}|} \tag{9}$$

There is also the possibility that purity could be the proportion of $|\mathbf{C}|$ to the resultant stimulus $|\mathbf{A}|$, that is, $P = |\mathbf{C}|/|\mathbf{A}|$. However, in vector mathematics, such a ratio is a cosine function (unless **C** and **A** are colinear), which is not linear. Thus, a scalar ratio would give a mathematically better behaved mixing function from 0 to 1. Letting the smallest color-matching function be the white component, a plot of the white component in the spectrum is given in Fig. 11. The peaks at 471 nm and 516 nm represent minimal perceptual purity. These occur also at the unique wavelengths in Fig. 10.

The points on the sides of the triangle of Fig. 10 can represent maximum (100%) purity. Thus, letting $|\mathbf{C}''|$ depict 100% purity at any wavelength, then the purity vector **P** in an appearance correlates according to (10), having direction θ from (6) since **P** and **C** are colinear.

$$\mathbf{P} = \frac{|\mathbf{C}|\ \mathbf{C}''}{|\mathbf{C}| + |\mathbf{W}|} \tag{10}$$

Accordingly, if there is no white component ($|\mathbf{W}| = 0$; 100% purity), only chroma contributes to luminance, which occurs above 540 nm since $\bar{z}_{10}$ is nearly zero. If $X = Y = Z > 0$, $|\mathbf{C}| = 0$, but $|\mathbf{W}| > 0$, and the response comprises only achromatic luminance (0 purity).

The MOTR model allows a very simple interpretation of the difference between *adding* white and increasing the white *level*. According to (2), *adding* white is equivalent to adding an amount w

to $\bar{x}_{10}$, $\bar{y}_{10}$, and $\bar{z}_{10}$. According to (4) and (6), neither the magnitude (chroma) nor direction (hue) of **C** is changed, but from (8), **A** appears lighter because as w is increased, |**W**| increases while |**C**| remains constant, thereby increasing |**A**| but also decreasing purity. To increase the white *level*, only the smallest tristimulus value ($\bar{z}_{10}$, for example, herein) is increased. From (4) and (5), as x' and y' decrease, |**C**| decreases, |**W**| increases, and thus purity decreases. From (7), the ratio of x" to y" would change (unless $\bar{x}_{10} = \bar{y}_{10}$), and a shift in hue (θ) should also occur. For stimuli with X, Y, or Z less than 100, white can be added with a concomitant increase in |**W**| but without a shift in hue until the largest tristim-ulus value reaches maximum (*i.e.*, 100), with a decrease in purity. Beyond this point, increasing the white *level* would reduce the **C** vector to zero along a curved path through hue shifts toward white. The hue shift should be small and masked even further by the rapidly increasing achromatic component.

Some distinction between purity and saturation in this model should be made, although many times, these two terms are used synonymously. The transformation of a set of tristimulus values X, Y, and Z according to (7) will always locate a point along the locus lines of Fig. 10 regardless of the purity or saturation of the stimulus. Different luminances (but less than that of the reference white) of a monochromatic yellow are all equally pure (100%), but the higher luminances will appear more "colorful", or more "saturated", than the lower ones. Thus, saturation might be used to to describe different purities of a hue, all at constant luminance, or different luminances of a hue at constant purity (colorfulness?). While purity as defined in (9) suggests the proportion of chroma in the stimulus at any luminance level, "saturation" commonly suggests the extent to which an *end point* is reached, and it would be nice to have colorimetric saturation defined quantitatively, ranging from 0 to 1 for any purity and luminance, suggesting a dependence on both. CIELUV saturation s_{uv} can be greater than 1, which again, makes conceptualization difficult. Perhaps "100% saturation" should be 100% purity *and* maximum luminance relative to white for a given hue. See Hunt [30] regarding colorfulness and saturation.

MOTR Model Purity Diagram

There seems a great preference for circular diagrams, perhaps due to the arrangement of Munsell hues in a nearly circular fash-

ion, and Fig. 9 or 10 can be easily transformed into a circle. Since Fig. 9 represents chroma vectors whose angle, not magnitude, determines hue, a hue circle can be created by simply dividing the chroma vector for each wavelength by its magnitude (normalization). Normalization creates a hue circle of unit radius, which is given in Fig. 12.

This normalization will place the hue of any color regardless of its chroma or purity on the circle's circumference. To make a circular purity diagram from Fig. 12, (10) is used, where $|\mathbf{C}''| = 1$. The circumference may then represent 100% purity of each hue. The normalized unit chroma vector for each wavelength is then multiplied by its purity so that $|\mathbf{P}| = P$ as given by (9). If this is done, Fig. 13 results. Most importantly, Fig. 13 is not a true chroma diagram because purity, not chroma, is the radial variable. If a chromaticity (*i.e.*, chroma and hue) diagram is desired, then chroma from (2) or (5) must be plotted, as in Fig. 9.

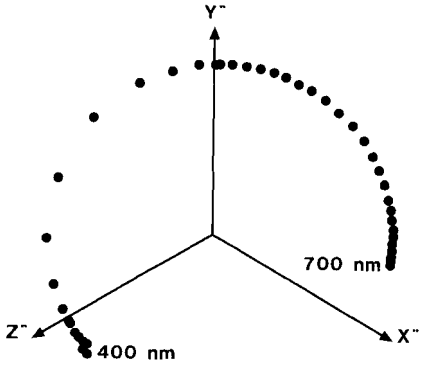

Fig. 12. Circular MOTR "hue" diagram of wavelengths in Figures 9 and 10.

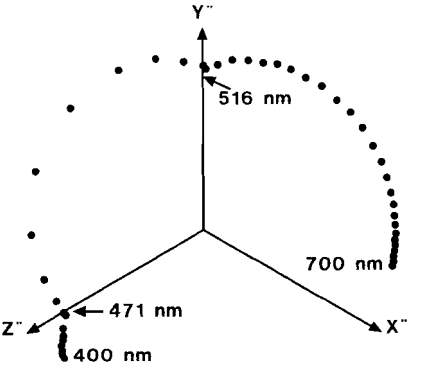

Fig. 13. Circular MOTR purity diagram of wavelengths in Figures 9 and 10.

A unit normalized purity diagram overcomes one difficulty with the 1931 CIE chromaticity diagram, where even for the wavelengths above 560 nm, the distance from the white point to the spectrum locus is not constant, even though all are "100% pure". In a sense, the 1931 CIE "chromaticity" diagram is really a hue diagram as in Fig. 10 in the region where $\bar{z}_{10}$ is 0, but is conceptually overall a "purity" diagram since no distance is based on pure chroma.

White Component

Thus far, the achromatic ("white") component W has been used without discussion as to how it might arise. While it is not intended to even speculate on a neurophysiological basis, speculation of a psychophysical model can be made. If the output of each axis in Fig. 8 is subtracted from its input, the result would be the value of the achromatic component. This subtraction could be done for only one tristimulus value or all three, with the result fed to a luminance channel along with the chromatic information as in (8). If appearance correlates with purity as in (9), it could suggest that the achromatic and chromatic signals are combined in a scalar mixing fashion to create the appearance response **A**, according to (8). The effect of other mathematical operations (*e.g.*, logarithmic) applied to these outputs will not be covered herein. Logarithmic or other monotonic functions (roots, exponentiation) will not change the unique hue aspects, but they do change the relative scaling and thus wavelength discrimination.

Surface Color Space

The color space for this model will incorporate many of the concepts in the CIE *xy*Y, L*a*b*, and L*u*v* spaces. The cube root L*a*b* system is somewhat empirical [28]. L*u*v* is also empirical but based on projective transformations [29, 30 (pp. 104-107)] of X, Y, and Z. A principal application for the MOTR model is graphic arts color reproduction, the subtractive, halftone printing process in particular. However, the MOTR model is also applicable to additive mixing processes as in color CRTs, etc.

From the data used for Figures 4, 5, and 7, Figures 14-18 can be derived. Figures 14-16 indicate chroma vs. dot area behavior. In Fig. 16 the chroma for the complementary colors plot on top of each other, which they should, since equal areas of ideal complementary colors should combine to a neutral as suggested in Fig. 7. The different chromas at 100% dot area mean that the visual chroma response is different for different pairs of complementary hues. The uppermost line is for the Y-B pair, the middle line is M-G, and the bottom line is R-C. Figures 14 and 15 produce different chroma responses for complementary colors, which increase with dot area. Since these are ideal colors, this behavior might not likely be found

with real colors, which lack the purity of the ideal colors, except possibly for dense, "clean" yellows. These ideal colors do not violate any physical laws and can be used as herein for elucidation purposes, but idiosyncratic behavior at their extreme chromas does not necessarily invalidate the color space used.

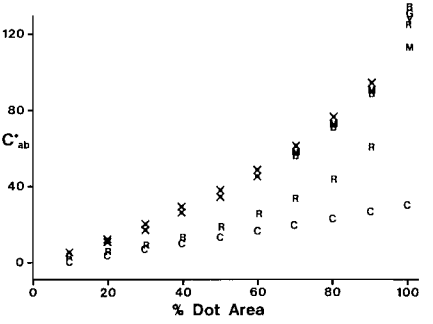

Fig. 14. C*ab vs. % dot area for ideal printing colors.

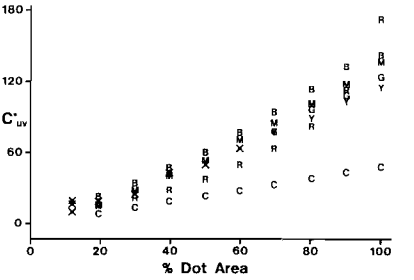

Fig. 15. C*uv vs. % dot area for ideal printing colors.

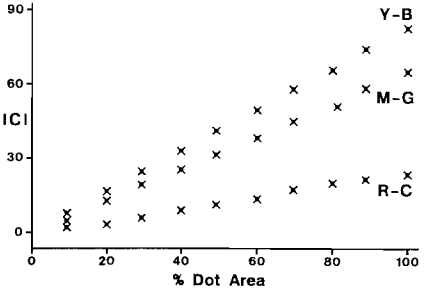

Fig. 16. MOTR |C| vs. % dot area for ideal printing colors.

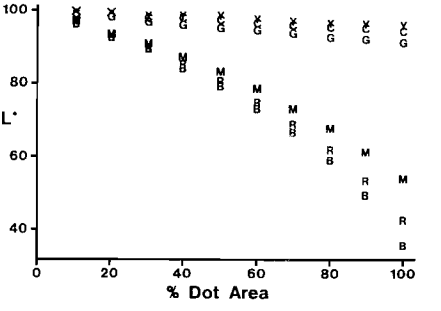

Fig. 17. CIE L* vs. % dot area for ideal printing colors.

The "lightness" characteristic for the CIE and MOTR spaces is shown in Figures 17 and 18. The lightness L* in Fig. 17 incorporates lightness due to both the achromatic and chromatic components. In Fig. 18, "W" represents the achromatic ("white") component in the color. In this regard, the MOTR space is really different. The MOTR space quantifies the chromatic and achromatic

components separately. This is advantageous for halftone printing, since the achromatic component can be treated separately as black, especially in complete gray component replacement (GCR).

A standard color space "test" is the depiction of Munsell colors, usually at constant Munsell Value, or lightness L*. A set of Munsell glossy chips of Hue = 5, Value = 6, with Chroma intervals (ΔC) of 2 was measured spectrophotometrically from 380 nm to 700 nm in 10 nm intervals via an integrating sphere with specular component excluded, and the color metrics calculated for CIE Illuminant C and the 2° Standard Observer, which is the standard viewing condition for Munsell samples. The color metrics for these chips in CIELAB and CIELUV are plotted in Figures 19 and 20. The point labelled "N" represents the neutral (achromatic) color V = 6.0. An ideal, uniform color space would desirably render these Munsell colors in radially symmetric, concentric circles. However, given the asymmetry of the CIE Standard Observer functions, it seems unreasonable to expect a color space to produce the spacing of visual perception as angularly symmetric, concentric circles. This is especially true in regard to hue (as dominant wavelength) because wavelength discrimination will correlate with the slopes of the Standard Observer color-matching functions as discussed earlier. Angular symmetry with dominant wavelength would require that wavelength discrimination is constant throughout the visible spectrum, which is quite obviously not true. Also, Munsell colors at a given V and C should not form a circle because it would mean that all hues of the same chroma have the same lightness. The luminous efficiency function $V(\lambda)$ shows this is not true.

A chroma diagram for these Munsell colors according to the MOTR model is given in Fig. 21. Fig. 21 is based only on the tristimulus values as per (2), so distance represents chroma, not purity. N is located away from the origin, indicative of the chromatic (bluish) effect of the Illuminant C. To "discount" the illuminant's chromatic effect (on perceived white) as is done in CIELAB and CIELUV, the tristimulus values are divided by the illuminant's tristimulus values as in CIELAB, which should place N at the origin and reference the other colors to this new origin. This occurs because in a vector space, a unitized basis set of vectors can be made by dividing each basis vector by its magnitude. In effect, this normalizes the data to a new "neutral" point.

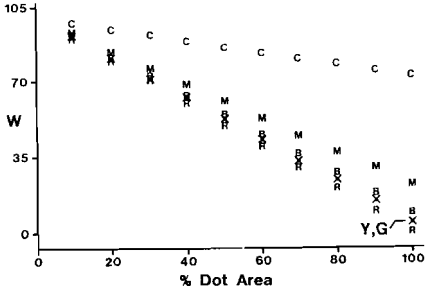

Fig. 18. W of MOTR model vs. % dot area of ideal printing colors.

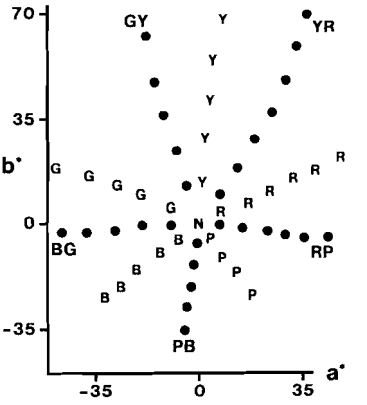

Fig. 19. CIE a*b* diagram of Munsell 5H hues at V=6 and ΔC=2.

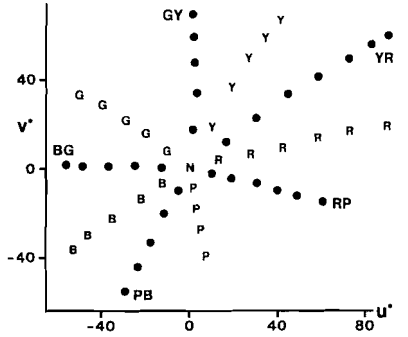

Fig. 20. CIE u*v* diagram of Munsell 5H hues at V=6 and ΔC=2.

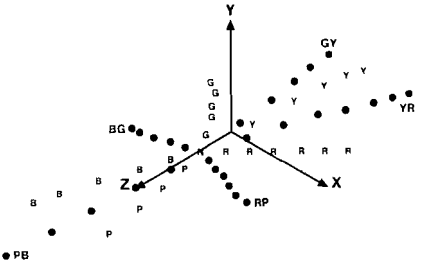

Fig. 21. MOTR chroma diagram of Munsell 5H hues at V=6 and ΔC=2.

The resulting data are plotted in Fig. 22. Note the angular "spread" from GY to BG, suggesting relatively low hue discrimination between these hues. The close spacing around Y and PB suggests higher hue discrimination there, since they represent "sensitive" (unique) hues. A large spread occurs also between the P and R hues, which correspond to the "purple line" of the CIE chromaticity diagram. There is no equivalent monochromatic wavelength in this region so the response should correspond more to color mixing than to monochromatic stimulation. In CIELAB and CIELUV

(Figures 19 and 20), Munsell Hue and Chroma "tend" to be uniformly spaced, although dominant wavelength (Hue) seems less uniformly spaced than Chroma. Fig. 22 is a truer "chromaticity" diagram than a*b* or u*v* diagrams because achromatic content is not included in Fig. 22's data points, and therefore, the radial spacing represents pure chroma differences. In CIELAB and CIELUV, the tristimulus values contain an achromatic component, although it is somewhat compensated for.

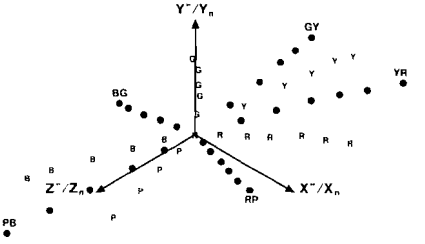

Fig. 22. MOTR "normalized" chroma diagram of Fig. 21.

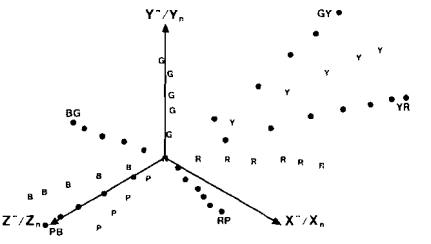

Fig. 23. MOTR "normalized" purity diagram of Fig. 21.

For halftone printing, a MOTR purity diagram is used instead of a chromaticity diagram. The reason is that halftone color printing is similar in concept to the 1931 CIE "chromaticity" diagram. In color printing, a DMax of an ink is mixed with the paper's white to produce tints. Black is added to produce shades. A given DMax can be considered 100% "purity" of that printed colorant so that tint scales represent purity scales relative to DMax. Applying this concept of purity to the data in Fig. 21, Fig. 23 results. While similar to Fig. 22, it tends to increase the radial spacings, especially expanding the G and GY hues, but the radial spacings still compress at the outer ends. However, there is still a question of what comprises the achromatic component **W** in the MOTR concept of purity.

The component $|\mathbf{C}|$ was the vector magnitude of only the chromatic components. Since X, Y, and Z contribute equally to the achromatic component, should $|\mathbf{W}|$ comprise the sum of the minimum X, Y, and Z values; *i.e.*, $3|\mathbf{W}|$, rather than only one tristimulus value as in (9)? If the magnitude of only one minimum tristimulus value is used, then the magnitudes of the other two are discarded from the computations as if they do not contribute. In CIELAB and CIELUV, all the tristimulus values are included. If

the other two tristimulus contributions are included, and purity is defined as in (11), Fig. 24 results, which gives more uniform radial spacing than Fig. 23, especially for the colors of high chroma. If the coefficient of $|\mathbf{W}|$ is varied for these Munsell chips, it is found that for values of the coefficient of $|\mathbf{W}|$ less than 3, the spacings compress at high chromas, and for values larger than 3, the spacings compress at low chromas. The application of (11) to Fig. 12 only accentuates the characteristics of Fig. 13 and doesn't change the qualitative aspects.

$$P = \frac{|\mathbf{C}|}{|\mathbf{C}| + 3|\mathbf{W}|} \tag{11}$$

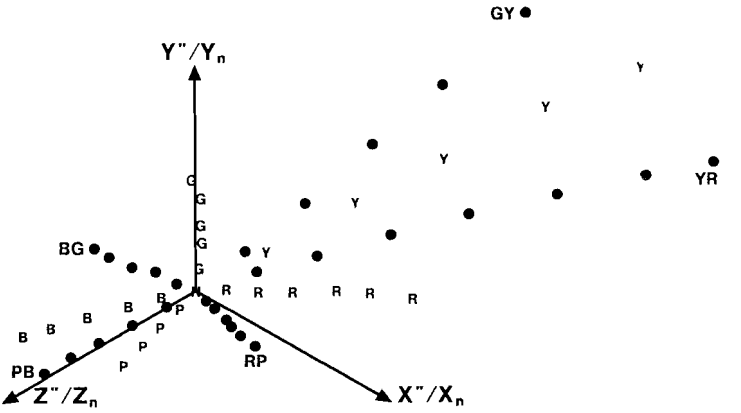

Fig. 24. MOTR "normalized" purity diagram of Fig. 23 based on a $3|\mathbf{W}|$ achromatic contribution.

An excellent example of the difference between using chroma and purity to represent color gradation in the graphic arts can be shown using tint scales of inks. In this case, gravure inks on standard paper stock were used. CIE tristimulus values were determined for Y, M, C, R, G, and B ink scales as for the Munsell samples, except that CIE Illuminant D50 was used, since this is the recommended viewing standard for graphic arts (See ISO #3664). The scales' CIE a*b* and u*v* diagrams are shown in Figures 25 and 26. The MOTR model purity diagram using $3|\mathbf{W}|$ is shown in Fig. 27. In both CIE diagrams, note that the blue (B) scale "hooks" back as its DMax is approached. This "J" shape suggests that some appearance aspect (chroma) of DMax is equivalent to about a 60% dot

area. However, what one sees in looking at the scales is a nearly monotonic change toward DMax, not a hooking. A nonperceptual overlapping of chroma without hooking as DMax is approached occurs more so for some colors (R, G, C) than others. A hooking suggests that a hue shift is occurring along with the compression. Such hooking and nonperceptual compression is absent in the MOTR purity diagram, although some curvature occurs. Some curvature, representing a hue shift, is expected since the color effect of the base rapidly diminishes as DMax is approached.

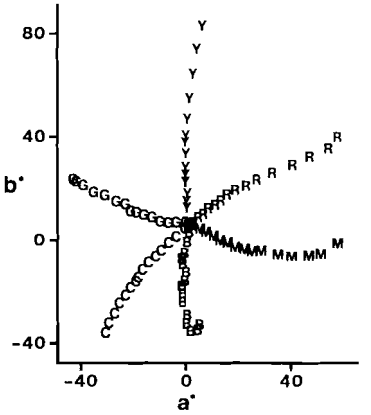

Fig. 25. CIE a*b* diagram of gravure ink scales.

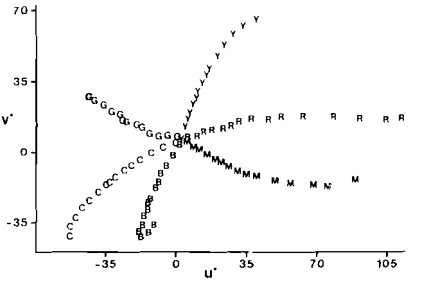

Fig. 26. CIE u*v* diagram of gravure ink scales.

The reason for these different behaviors is that the CIE diagrams represent *chroma*, which does decrease as a high DMax is approached, especially for darker colors. However, the achromatic level is also decreasing so that what one perceives is the combined effect of a change in both chroma and lightness. The MOTR purity diagram shows the combined effect of chromatic *and* achromatic components, which is what correlates perceptually. If a MOTR chroma diagram is made, it will behave similarly to the CIE diagrams because chroma decreases in the MOTR model also. Thus, the MOTR model purity approach seems better for visual representation in the graphic arts.

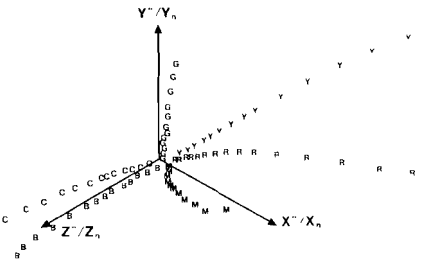

Fig. 27. MOTR model purity diagram of gravure ink scales.

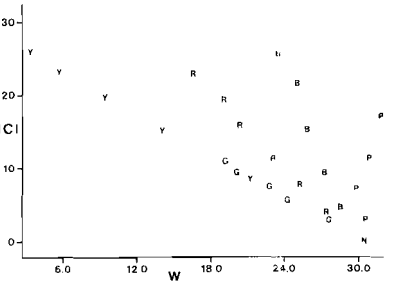

Fig. 28. MOTR | **C** | vs. W for Munsell 5H hues, V=6, ΔC=2.

The MOTR Model and GCR

A more important advantage of the MOTR model is its applicability to halftone color reproduction since it intrinsically reduces any color to two chromatic components and one achromatic one, which is particularly advantageous to complete GCR. Another intrinsic advantage is its linearity of W with dot area (Fig. 19). It has an advantage also regarding lightness L*. If | **C** | is plotted against W for the Munsell colors, Fig. 28 results. There is a linear relation between MOTR chroma and achromatic components. Since these Munsell colors all have the same lightness, Fig. 28 suggests the lightness of a color can be separated into *linear* combinations of MOTR chroma and W without a change in lightness, as was suggested in (8). The CIE spaces cannot do this. Thus, in the MOTR model, large data tables are not necessary since only the parametrics to define a straight line for each producible hue have to be stored.

To use the MOTR model to determine a 100% GCR composition, one first determines the hue and chroma of the original color in MOTR model parameters and CIE lightness L*. From empirical tables, the appropriate combination of two primaries to produce the desired hue is selected. From the value of lightness L* required, the | **C** | vs. W parameters for that lightness are selected. From the values of the chroma produced by the two primaries and the chroma of the color to be reproduced, the remaining lightness contribution by the achromatic level is easily determined. Since these tables can be in terms of linear parameters of dot area, storage of data is signifi-

cantly reduced. More importantly, the color representations develop naturally from appearance derived color-matching functions, not arbitrary transformations or empirical mathematical "best fits", thereby enhancing the likelihood of achieving matches to appearance without extensive iterations of color correction.

Although it was said that black is added to the *colors*, it is more useful if it is considered that black is added to the *base*. One can view this as adding the same, highly "pure" ink to a paper with some gray level. The principal purpose of adding black is to extend the color gamut to lower L* values. However, a secondary effect of adding black is to decrease the maximum possible chroma, even though the purity might be 100%. This effect is similar to that discussed for Fig. 3. Since in shade scales, black is added to the colors, it is as if the colors are placed on a neutral base having an achromatic level corresponding to the amount of black. Thus, it is necessary to know the lightness L* vs. black area of the paper to be printed on. The MOTR model uses the achromatic component only for lightness scaling so that lightness can be altered without a shift in hue. This conceptual difference in the use of lightness in color reproduction is the greatest difference in the MOTR model and the CIE spaces. The CIE a*b* and u*v* diagrams are best for applications at constant lightness as in Munsell Value planes. When lightness and chroma both change significantly, color systems representing only chroma changes won't correlate well visually, since people will perceive the combined effect of both changes. Besides the Munsell system, the MOTR model gives far better visual representations of both the Swedish NCS and German DIN systems than CIELAB and CIELUV do.

Color Difference

The principal intent of the CIELAB and CIELUV systems is to provide a quantitatively objective means to calculate small color differences which correlate well with visual differences. Another earlier approach by MacAdam [31] for acceptable/detectable color differences used ellipses, and this approach remains today also as a principal method. In fact, such ellipses are usually called "MacAdam ellipses". In general, the 1931 CIE chromaticity coordinates are used, but CIELAB and CIELUV coordinates can also be used [32-38]. A more mathematical approach is that proposed by Helmholtz using the color space geometry in line elements of Rie-

mannian space [39-43]. For a general discussion, see Wyszecki and Stiles [44, Ch. 8.4]. In a chromaticity plane where chromaticity discrimination can be described by an ellipse, the color metric for the chromaticity difference ΔC can be given as in (12), where g_{11}, g_{12}, and g_{22} are the metric coefficients [39], and Δx and Δy are the coordinate differences of the color in the orthogonal CIE x,y chromaticity plane. MacAdam [39] was able to show that where chromaticity discrimination plotted as an ellipse in CIE chromaticity coordinates, the same data plotted as a circle when the x and y axes were at an angle of about 133°. This is a standard mathematical procedure to determine a new set of axes such that $g_{12} = 0$.

$$(\Delta C)^2 = g_{11}(\Delta x)^2 + 2g_{12}(\Delta x)(\Delta y) + g_{22}(\Delta y)^2 \tag{12}$$

In a multiple linear regression analysis of a color metric using differences in the opponent-color tristimulus values X*, Y*, and Z* with and without cross-product terms, Rich [41] stated, "The only reasonable conclusion ... is that there seems to be a need to include the cross-product terms in the model. The results ... indicated ... that the addition of the cross-product terms would increase the correlation between the calculated and visual scales." Thus, a non-orthogonal chromaticity plane would seem to provide a better correlation between visual and calculated color differences.

In the MOTR model, in the $\mathbf{X}''$,$\mathbf{Y}''$ tridant, for example, from (3) the magnitude of an origin-bounded vector would be given by (13), and the magnitude of any difference between points in this tridant would be given by (14). A difference between points in two tridants would require the analogous use of (3) in all variables. If $|\mathbf{C}|$ is a constant, (3) defines a circle in planar trigonal coordinates, and, therefore, (14) would define a circle about the reference point (x''_0, y''_0) with radius $\Delta\mathbf{C}$. Thus, the planar geometry of this model produces a circular color metric for constant chromaticity differences.

$$|\mathbf{C}|^2 = x''^2 - x''y'' + y''^2 \tag{13}$$

$$(\Delta\mathbf{C})^2 = (x''_1 - x''_0)^2 - (x''_1 - x''_0)(y''_1 - y''_0) + (y''_1 - y''_0)^2 \tag{14}$$

The discrimination data from Rich and Billmeyer [42] for a yellow color center based on the 10° CIE Standard Observer are

shown in Fig. 29. Using the CIE tristimulus values for these data, the corresponding distribution of visual responses according to a MOTR model purity diagram is given in Fig. 30, where the reference point is not at the origin. The *shapes* of the two distributions are virtually identical. Thus, the color metric of the MOTR model space seems equivalent to color metrics in Riemannian space. However, much more investigation would be needed to verify this ability.

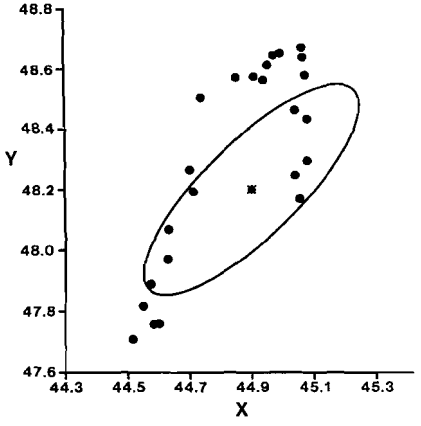

Fig. 29. Color difference data of Rich & Billmeyer, Jr. [42].

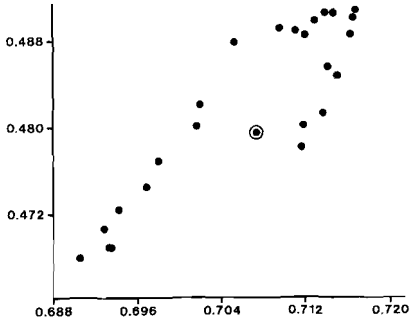

Fig. 30. MOTR model purity diagram of data in Fig. 29.

Selected Bibliography

1. T. Young, "On the Theory of Light and Colors", *Phil. Trans. Royal Soc. London*, **92**, pp. 20–71 (1802).*

2. J. C. Maxwell, "Theory of the Perception of Colors", *Trans. Royal Scottish Soc. Arts*, **4**, pp. 394–400 (1856).*

3. J. C. Maxwell, "The Diagram of Colors", *Trans. Royal Soc. Edinburgh*, **21**, pp. 275–298 (1857).*

4. J. C. Maxwell, "Theory of Compound Colors, and the Relations of the Colors of the Spectrum", *Proc. Royal Soc. London*, **10**, pp. 404–409 (1860).*

5. J. C. Maxwell, "On Color Vision", *Proc. Royal Inst. Great Brit.*, **6**, pp. 260–271 (1872).*

6. H. von Helmholtz, "Versuch einer erweiterten Anwendung des Fechnerschen Gesetzes im Farbensystem", *Z. Psychol. Physiol. Sinnesorg.*, **2**, pp. 1–30 (1891).

7. H. von Helmholtz, *Handbuch der Physiologischen Optik*, 2nd. Ed., Voss, Hamburg, 1896.*

8. E. Hering, *Zur Lehre vom Lichtsinne*, (1878); *Outlines of a Theory of the Light Sense*, a translation by L. M. Hurvich and D. Jameson, Harvard U. Press, 1964.

9. R. W. Massof, J. F. Bird, "A General Zone Theory of Color and Brightness Vision. I. Basic Formulation", *J. Opt. Soc. Am.*, **68**, No. 11, pp. 1465–1471 (1978).

10. J. F. Bird, R. W. Massof, "A General Zone Theory of Color and Brightness Vision. II. The Space-Time Field", *ibid.*, pp. 1471–1481 (1978).

11. R. W. Massof, "Color-Vision Theory and Linear Models of Color Vision", *Color Res. & Appl.*, **10**, No. 3, pp. 133–146 (Fall 1985).

12. C. R. Ingling, Jr., B. H. Tsou, "Orthogonal Combination of Three Visual Channels", *Vision Res.*, **17**, pp. 1075–1082 (1977).

13. S. L. Guth, R. W. Massof, T. Benzschawel, "Vector Model for Normal and Dichromatic Color Vision", *J. Opt. Soc. Am.*, **70**, No. 2, pp. 197–212, (Feb. 1980).

14. D. L. MacAdam, "The Theory of the Maximum Visual Efficiency of Colored Materials", *ibid.*, **25**, pp. 249–252 (Aug. 1935).

15. D. L. MacAdam, "Maximum Visual Efficiency of Colored Materials", *ibid.*, pp. 361–367 (Nov. 1935).

16. K. McLaren, "CIELAB Hue-Angle Anomalies at Low Tristimulus Ratios", *Color Res. & Appl.*, **5**, No. 3, pp. 139–143 (Fall 1980).

17. E. Q. Adams, "X-Z Planes in the 1931 I.C.I. System of Colorimetry", *J. Opt. Soc. Am.*, **32**, pp. 168–173 (March 1942).

18. E. Q. Adams, "A Theory of Color Vision", *Psychol. Rev.*, **36**, pp. 56–76 (1923).

19. F. L. Dimmick, M. R. Hubbard, "The Spectral Location of Psychologically Unique Yellow, Green, and Blue", *Amer. J. Psychol.*, **52**, pp. 242–254 (1939).

20. F. L. Dimmick, M. R. Hubbard, "The Spectral Components of Psychologically Unique Red", *ibid.*, pp. 348–353 (1939).

21. V. C. Smith, J. Pokorny, "Spectral Sensitivity of Color-Blind Observers and the Cone Photopigments", *Vision Res.*, **12**, pp. 2059–2071 (1972).

22. O. Estevez, "On the Fundamental Data-Base of Normal and Dichromatic Colour Vision", Ph.D. Thesis, U. of Amsterdam (see Hunt [24], Table 1).

23. R. M. Boynton, "A System of Photometry and Colorimetry Based on Cone Excitations", *Color Res. & Appl.*, **11**, pp. 244–252 (Winter 1986).

24. R. W. G. Hunt, "A Model of Colour Vision for Predicting Colour Appearance", *ibid.*, **7**, Part 1, pp. 95–112 (Summer 1982).

25. R. W. G. Hunt, M. R. Pointer, "A Colour-Appearance Transform for the CIE 1931 Standard Colorimetric Observer", *ibid.*, **10**, No. 3, pp. 165–179 (Fall 1985).

26. R. E. Bedford, G. W. Wyszecki, "Wavelength Discrimination for Point Sources", *J. Opt. Soc. Am.*, **48**, pp. 129–135 (1958).

27. K. J. McCree, "Small Field Tritanopia and the Effects of Voluntary Fixation", *Optica Acta*, **7**, pp. 317–323 (1960).

28. L. G. Glasser, A. H. McKinney, C. D. Reilly, P. D. Schnelle, "Cube-Root Color Coordinate System", *J. Opt. Soc. Am.*, **48**, 10, pp. 736–740 (Oct. 1958).

29. D. L. MacAdam, "Projective Transformations of I.C.I. Color Specifications", *ibid.*, **27**, pp. 294–299 (Aug. 1937).

30. R. W. G. Hunt, *The Reproduction of Colour*, 4th Ed., Van Nostrand-Reinhold, 1988.

31. D. L. MacAdam, "Visual Sensitivities to Color Differences in Daylight", *J. Opt. Soc. Am.*, **32**, pp. 247–274 (1942).

32. W. R. J. Brown, D. L. MacAdam, "Visual Sensitivities to Combined Chromaticity and Luminance Differences", *ibid.*, **39**, No. 10, pp. 808–834 (Oct. 1949).

33. H. R. Davidson, E. Friede, "The Size of Acceptable Color Differences", *ibid.*, **43**, No. 7, pp. 581–589 (July 1953).

34. G. Wyszecki, G. H. Fielder, "New Color-Matching Ellipses", *ibid.*, **61**, No. 9, pp. 1135–1152 (Sept. 1971).

35. N. Ohta, "Correspondence Between CIELAB and CIELUV Color Differences", *Color Res. & Appl.*, **2**, No. 4, pp. 178–182 (Winter 1977).

36. R. C. Zeller, H. Hemmendinger, "Evaluation of Color-Difference Equations: A New Approach", *ibid.*, **4**, No. 2, pp. 71–77 (Summer 1979).

37. R. G. Kuehni, "Advances in Color-Difference Formulas", *ibid.*, **7**, No. 1, pp. 19–23 (Spring 1982).

38. R. M. Boynton, A. L. Nagy, C. X. Olson, "A Flaw in Equations for Predicting Chromatic Differences", *ibid.*, **8**, pp. 69–74 (Summer 1983).

39. D. L. MacAdam, "Specification of Small Chromaticity Differences", *J. Opt. Soc. Am.*, **33**, pp. 18–26 (1943).

40. R. M. Rich, F. W. Billmeyer, Jr., "Method for Deriving Color-Difference-Perceptibility Ellipses for Surface Color Samples", *J. Opt. Soc. Am.*, **65**, No. 8, pp. 956–959 (Aug. 1975).

41. D. C. Rich, "A Color Metric from Opponent-Color Visual Channels", *Color Res. & Appl.*, **5**, No. 2, pp. 76–80 (Summer 1980).

42. D. C. Rich., F. W. Billmeyer, Jr., "Small and Moderate Color Differences. IV. Color-Difference-Perceptibility Ellipses in Surface-Color Space", *ibid.*, **8**, No. 1, pp. 31–39 (Spring 1983).

43. D. L. MacAdam, "Metric Coefficients for CIE Color-Difference Formulas", *ibid.*, **10**, No. 1, pp. 45–49 (Spring 1985).

44. G. Wyszecki, W. S. Stiles, *Color Science: Concepts and Methods, Quantitative Data and Formulae*, 2nd Ed., Wiley, 1982.

45. J. B. Cohen, "Color and Color Mixture: Scalar and Vector Fundamentals", *Color Res. & Appl.*, **13**, No. 1, pp. 5–39 (Feb. 1988).

* Reprinted in part or in entirety in *Sources of Color Science* by D. L. MacAdam, MIT Press, 1970.